Gädda, A.; Ott, Jennifer; Bharthuar, S.; Brücken, Erik; Kalliokoski, Matti; Karadzhinova-Ferrer, A.; Bezak, M.; Kirschenmann, S.; Litichevsky, V.; Golovleva, M.; Martikainen, Laura; Winkler, Alexander; Chmill, V.; Tuovinen, E.; Luukka, P.; Härkönen, Jaakko

AC-coupled n-in-p pixel detectors on MCz silicon with atomic layer deposition (ALD) grown thin film

Published in:
NUCLEAR INSTRUMENTS AND METHODS IN PHYSICS RESEARCH SECTION A: ACCELERATORS SPECTROMETERS DETECTORS AND ASSOCIATED EQUIPMENT

DOI:
10.1016/j.nima.2020.164714

Published: 11/01/2021

Document Version
Peer-reviewed accepted author manuscript, also known as Final accepted manuscript or Post-print

Please cite the original version:
Gädda, A., Ott, J., Bharthuar, S., Brücken, E., Kalliokoski, M., Karadzhinova-Ferrer, A., Bezak, M., Kirschenmann, S., Litichevsky, V., Golovleva, M., Martikainen, L., Winkler, A., Chmill, V., Tuovinen, E., Luukka, P., & Härkönen, J. (2021). AC-coupled n-in-p pixel detectors on MCz silicon with atomic layer deposition (ALD) grown thin film. *NUCLEAR INSTRUMENTS AND METHODS IN PHYSICS RESEARCH SECTION A: ACCELERATORS SPECTROMETERS DETECTORS AND ASSOCIATED EQUIPMENT*, *986*, Article 164714. https://doi.org/10.1016/j.nima.2020.164714

Journal Pre-proof

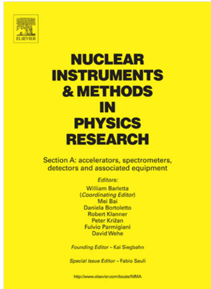

AC-coupled n-in-p pixel detectors on MCz silicon with atomic layer deposition (ALD) grown thin film

A. Gädda, J. Ott, S. Bharthuar, E. Brücken, M. Kalliokoski, A. Karadzhinova-Ferrer, M. Bezak, S. Kirschenmann, V. Litichevsky, M. Golovleva, L. Martikainen, A. Winkler, V. Chmill, E. Tuovinen, P. Luukka, J. Härkönen

PII: S0168-9002(20)31111-6
DOI: https://doi.org/10.1016/j.nima.2020.164714
Reference: NIMA 164714

To appear in: *Nuclear Inst. and Methods in Physics Research, A*

Received date : 29 February 2020
Revised date : 15 September 2020
Accepted date : 17 September 2020

Please cite this article as: A. Gädda, J. Ott, S. Bharthuar et al., AC-coupled n-in-p pixel detectors on MCz silicon with atomic layer deposition (ALD) grown thin film, *Nuclear Inst. and Methods in Physics Research, A* (2020), doi: https://doi.org/10.1016/j.nima.2020.164714.

AC-coupled n-in-p pixel detectors on MCz silicon with atomic layer deposition (ALD) grown thin film

A. Gädda[a,b], J. Ott[a,c], S. Bharthuar[a], E. Brücken[a], M. Kalliokoski[a], A. Karadzhinova-Ferrer[d], M. Bezak[d], S. Kirschenmann[a], V. Litichevsky[a,e], M. Golovleva[a,f], L. Martikainen[a], A. Winkler[a,g], V. Chmill[d], E. Tuovinen[b], P. Luukka[a,f], J. Härkönen[d]

[a] *Helsinki Institute of Physics, Gustaf Hällströmin katu 2, 00014 University of Helsinki, Finland*
[b] *Advacam Oy, Tietotie 3, 02150, Espoo, Finland*
[c] *Aalto University, Department of Electronics and Nanoengineering, Tietotie 3, 02150 Espoo, Finland*
[d] *Ruđer Bošković Institute, Bijenička cesta 54, 10000 Zagreb, Croatia*
[e] *Specom Oy, Tekniikantie 2A 326, 02150, Espoo, Finland*
[f] *Lappeenranta-Lahti University of Technology LUT, Yliopistonkatu 34, 53850 Lappeenranta, Finland*
[g] *Detection Technology Plc, A Grid, Otakaari 5A, 02150 Espoo, Finland*

Abstract

We report initial characterization of our novel sensor process solutions with AC-coupled $n^+/p^-/p^+$ pixel detectors made on 150 mm diameter p-type Magnetic Czochralski silicon (MCz-Si) wafers. The pixels were segmented in a 52 × 80 dual column array and designed to be AC capacitive coupled. The resistive coupling between pixels, allowing quality assurance probing prior the flip chip bonding, was realized with thin film metal-nitride resistors fabricated by sputtering deposition. This approach allows us to omit punch-through resistor structures, which reduces the overall process complexity. Moreover, our previous studies have emphasized that applying ALD Aluminum Oxide (Al_2O_3) field insulator and passivation layer results in negative net oxide charge and thus additional p-spray or p-stop surface current termination structures are not necessary. Our focused application is a radiation-hard ALD AC-coupled pixel detector to be used in future particle physics experiments, such as the High-Luminosity Large Hadron Collider (HL-LHC), as well as photon counting applications. The pixel detectors were tested at Helsinki Institute of Physics (HIP) Detector laboratory and Ruđer Bošković Institute (RBI). We show measurement

Email address: akiko.gadda@helsinki.fi (A. Gädda)

data of pixel detectors and other test structures. For the TiN resistors surrounding pixels, the resistance values were measured to be about 15 kΩ. Data of electrical properties, full depletion voltage and leakage current are shown as well. Our Transient Current Technique (TCT) measurements indicated clear pixel segmentation with excellent homogeneity. For further study, AC-coupled sensors were hybridized to PSI46dig read out chips (ROC) by flip-chip interconnection technique and tested with a radioactive source.

Keywords: Pixel Detector, Magnetic Czochralski Silicon, Atomic Layer Deposition, Flip Chip Bonding

---

1. Introduction

Pixel detectors made of silicon are frequently used for particle tracking applications at different high-energy physics experiments. In CERN HL-LHC, an extensive amount of Si modules will be installed [1–3]. Thus, the use of Si material is pertinent from both the material as well as the production cost perspective. Amongst the Si materials, Magnetic Czochralski silicon (MCz-Si) is a potentially radiation hard detector material due to its higher oxygen concentration with respect to traditionally used Float Zone silicon (Fz-Si) materials. The concentration of oxygen in MCz-Si is about 5-10$\times10^{17}$cm^{-3} and it can be adjusted by magnetic field in the growing process [4]. The higher oxygen concentrations in high-resistivity MCz-Si wafer enables the formation of shallow-level defects known as thermal donors (TDs). These can also be introduced on purpose, in order to compensate the acceptor doping and thus tailor the full depletion voltage (V_{fd}) of the Si sensor. Also proton radiation deterioration has been shown to have less impact on sensors processed on this material [5].

There is a strong motivation for the use of p-type Si. Conventionally, n-type Si wafers are used as the detector material. A disadvantage of n-type detectors is the Space Charge Sign Inversion (SCSI) effect that tends to appear after irradiation with high fluences. This causes a decreased sensitivity of the detector. On the other hand, a detector made of p-type Si is not only expected to eliminate the SCSI problem, but also can reach higher charge collection efficiency (CCE). However, in this configuration the positive oxide charge in SiO_2 becomes an issue. The accumulation of surface electron charges results in poor spatial resolution. Thus, a p-spray or p-stop implantation step has to be added in the Si detector process. In this paper, we applied thin film oxidation insulator instead of conventional SiO_2. Especially, the thin film grown by atomic layer deposition (ALD) is recognized as an attractive approach as semiconductor processing technique. Coating with ALD aluminium oxide (Al_2O_3)

provides a field insulator providing natural surface current termination due to its well-known negative oxide charge property [4, 6–9]. By replacing SiO_2 with ALD Al_2O_3, we can omit the p-spray or p-stop process steps.

An AC-coupled detector design has the benefit that a signal can be separated from leakage current. The signal current from an incident particle can be propagated to the readout electronics through a pixel capacitor, while the leakage current flows to the common bias line via a bias resistor fabricated in the peripheral area of the pixel areas. Our AC-coupled structure consists of an Al_2O_3 insulation layer between the implanted silicon substrate and the pixel electrode. In this study we applied a thin film ALD aluminum oxide as the insulation material and sputtered Titanium Nitride (TiN) as the biasing resistor material.

For characterization of the fabricated sensors we used Transient Current Technique (TCT), which is a commonly adopted method [10–12]. Especially, observation of the charge collection behavior with the good spatial resolution provided by modern laser systems can confirm the success in sensor fabrication [13], if for example a dedicated readout ASIC is not available. Both electrons and holes contribute to the induced current. Furthermore, short wavelength laser TCT gives us information about the efficiency of our sensors for short range particles such as alpha particles or other ions possibly emitted from nuclear materials. In addition, 1060 nm IR laser TCT characterizes the effectiveness of our pixel sensors for Minimum Ionizing Particles (MIP) which are present in scientific High Energy Physics (HEP) and astrophysics experiments.

To validate the functionality of our AC-coupled pixel detector, we hybridized the sensor to the CMS PSI46dig read-out chip (ROC) [14] by flip-chip bonding (FCB). For this purpose, under-bump metalization (UBM) based on a TiW/Au metal stack was prepared on the sensors. The hybridized detector assemblies were then tested with radioactive sources, most importantly Am-241.

2. Detector processing

A 320 µm thick boron doped p-type 150 mm MCz-Si wafer with resistivity $4-8$ kΩcm from Okmetic Oyj was processed at Micronova Nanofabrication Center in Espoo, Finland. First, a 300 nm thick dry oxide (SiO_2) layer was grown in oxidation furnace (PEO Centrotherm) at peak temperature of 1100 °C. The first photolithography was for alignment marks on the Si surface. The standard alignment marks were exposed using a stepper (FPA3000-i4 Canon). The oxide layer and Si were etched using an oxide etcher (LAM Oxford). The use of helium cooling gas was reduced to avoid risk of wafer breakage. The depth of the alignment marks on Si was 100 nm. After the Si dry etching, the photo resist was removed, and a second photolithography step was carried out. The implantation opening pattern was transfered to the existing thermal oxide layer by using buffered oxide etcher (BOE) as known as buffered hydrogen fluoride (BHF) wet etching. After the wet etching, the existing photo resist was removed. Then ion implantation step was carried out with the patterned thermal oxide hard mask. On the front side, phosphorus was implanted by an ion implanter (Eaton 8200) with the voltage of 60 kV and total dose of $10^{15}/\mathrm{cm}^3$. Similarly, boron field implantation was conducted using the voltage of 20 kV on the backside of the wafer. A yield in junction depth of approximately 3 µm was expected.

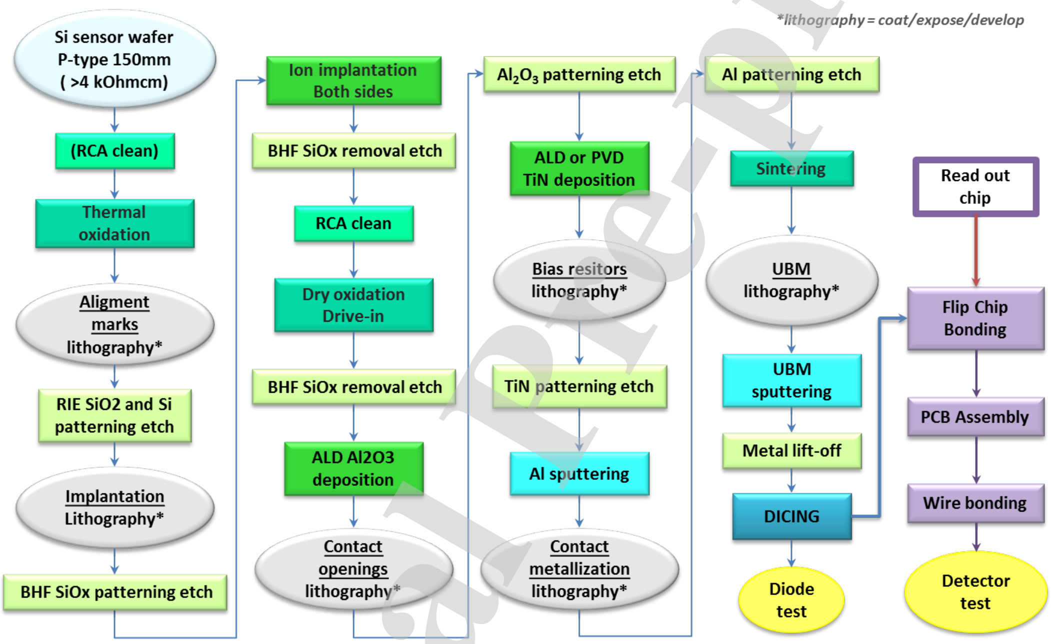

Figure 1: Process flow for AC-coupled pixel detectors on MCz silicon with ALD grown thin film.

After removing the hard mask by BOE, the wafers were cleaned using the Radio Corporation of America (RCA) cleaning process. Consequently, the implants were activated by thermal diffusion into the bulk Si, called drive-in step in the oxidation furnace. The activation step again deposits a thin layer of the oxide of approximately 100 nm, this was removed using the BOE bath. An insulation layer was deposited using ALD. The detailed steps of the ALD deposition are described in [15, 16] . The Al_2O_3 insulation layer was patterned by wet etching in an aluminum etching bath. Then a TiN bias resistor was deposited with a physical vapor deposition (PVD) RF sputtering (Von Ardenne). The TiN film was patterned using hydrogen peroxide

(H_2O_2). After the thin film deposition processes, aluminum metal was deposited both front and backside using PVD DC sputtering (Von Ardenne). The backside metal was protected with a photo resist while patterning the pixel contact metal on the front side in the aluminum etching bath. The pixel detector configuration requires hybridization of the sensor and ROC by FCB technique. The ROC has SnPb solder bumps deposited by Advacam Oy. The solder wetting metal is required on the surface of a sensor side. Thus the UBM was prepared using PVD sputtering (MRC Mark-II). Tungsten-titanium (TiW) of 20 nm thickness as an adhesion metal layer followed by gold (Au) of about 200 nm thickness as a solder wetting metal were deposited. The UBM patterning was done by the metal lift-off technique. In this report, we diced the wafer before the UBM metallization step, because our design includes multiple other test structures, MOS capacitors and diodes, which do not require UBM. In other words, any further steps which may interfere with the surface structure and measurement of these other devices at this phase were avoided. During the FCB step, the PSI46dig ROC and sensor were pre-aligned by the optics equipped in the FCB tool (FC150 SET). Figure 2 shows the cross sectional drawing of the AC-coupled Si pixel detector. The provided value of the post bonding accuracy form the tool manufactures is higher than 3 µm. In this study, we used a flux-less thermo-compression bonding which is controlling temperature and force while the pixel solder bumps establish the electrical connections. An eutectic point of a SnPb solder is about 184 °C, applying the temperature with appropriate force, imposed range of 50-100 mg/bump, can establish the bump bond connections together with a reflow step. Also, another parameter leveling is an important sequence during the alignment procedure. We used an autocollimator installed in the optical unit adjusting the parallelism between the ROC and sensor surfaces.

The processed thin film TiN bias resistor thickness was measured under the optical profilometer (Vision 64 Burker). The measured bias thickness was 37 nm (see Figure 3). The average sheet resistance of the TiN thin film was measured to be 54 Ω/sq, with a variation of up to 15 % over the wafer. This variation might be caused by a variation in thickness at the position of the wafer, as is not unusual in sputter deposition. Non-stoichiometric nitride film resistivity may also be affected by the deposition tool. Although this study is focused on research providing a proof of concept, a tool that was not available due to the technical reasons during this study, such as ALD, may endorse a better film and uniformity.

The resistance value for an individual pixel resistor was around 15 kΩ. This is lower than presented in one of our previous reports, where resistances of 0.1 MΩ and 0.08 MΩ for 12 nm and 23 nm thick TiN resistor structures grown by ALD were determined, respectively [4]. As expected, the resistance of the TiN film is decreased

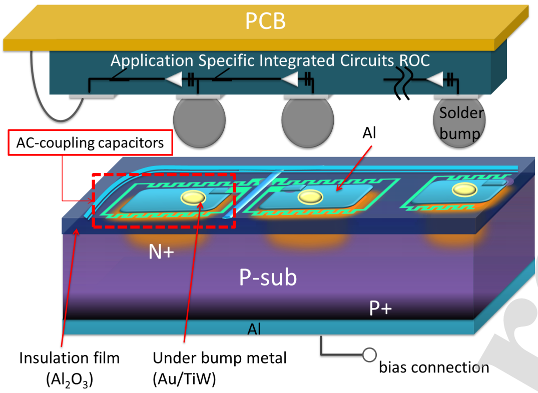

Figure 2: A schematic drawing of the AC-coupled Si pixel detector: ROC having solder bumps (above) and sensor (bottom).

as film thickness increases, and resistance remains low when the sample is annealed in non-oxidizing conditions. To bias the detector even at higher leakage currents without significant voltage drop, a slightly lower value of the bias resistor is in fact favorable.

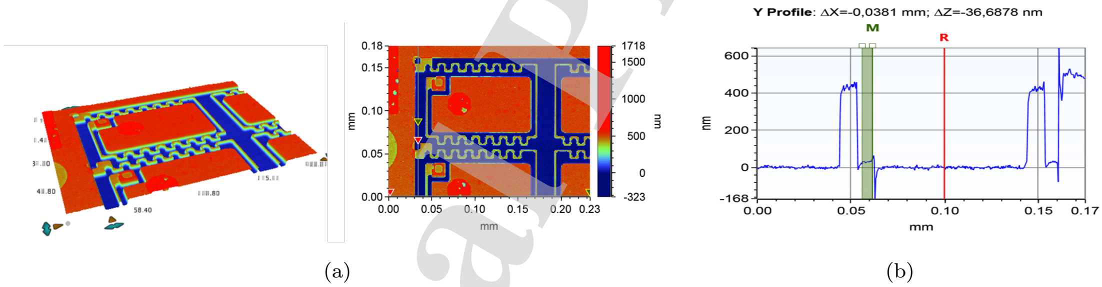

Figure 3: (a) Optical profilometer maps of TiN bias resistor structure around a pixel, (b) height profile with resistor highlighted in green.

3. Transient Current Technique Measurement

Different types of pixel sensors on our wafer were characterized with the TCT setup (Particulars d.o.o [17]) at the Detector Laboratory in Helsinki Institute of Physics (HIP) and at the Laboratory in Ruđer Bošković Institute (RBI). Both facilities have identical basic setups that consist of a pulsed laser source, optics with an adjustable diaphragm collimator, and a sample holder with an XYZ-stage [18, 19]. The diced $n^+/p^-/p^+$ sensor was attached to the measurement setup, and provided with bias voltage from a Keithley 2410 SourceMeter to the the back plane of the sensor chip. The signals were read from front side of the chip on a corner bias contact pad with the help of a contact needle.

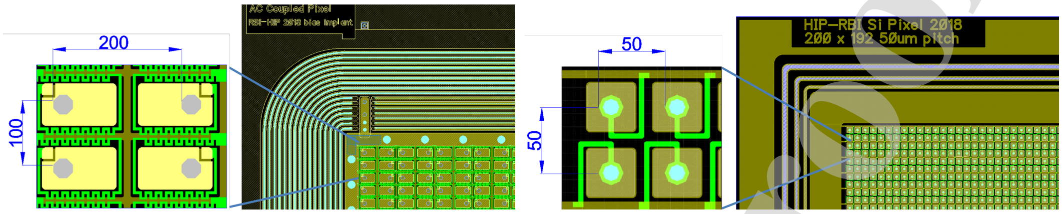

(a) (b)

Figure 4: Two types of pixel sensor designs: (a) PSI46dig-geometry AC-coupled pixel sensor with 100 µm × 150 µm pitch (b) RD53A-geometry DC-coupled pixel sensor with 50 µm × 50 µm pitch.

Measurements were performed at room temperature and the wavelength of λ = 670 nm for red laser and λ = 1064 nm for infrared laser were set with a repetition rate of 50 Hz. The two types of the sensors shown in Figure 4 were measured. In the Figure, the left hand side (a) shows a mask design of PSI46dig sensor (52 × 80 pixel matrix) and the right hand side (b) shows a design of RD53A sensor (400 × 192 pixel matrix). For (a) sensor, the applied bias voltage was 80 V. An area of 500 × 500 µm^2 was selected to produce a spatial homogeneity scan with a resolution of 5 µm. The CCE is defined as an integral over the TCT signal with a 25 ns time window. The transient signal is normalized by using the highest value of collected charged due to the measured signal in the scanned area. For the (b) sensor, the applied bias voltage was 100 V and an area of 1000 × 1000 µm^2 was scanned. The pitch between two bump openings is 50 µm, i.e. the size of the metallization on n$^+$ pixel is about 38 µm × 38 µm. The gap between the metals was 12 µm.

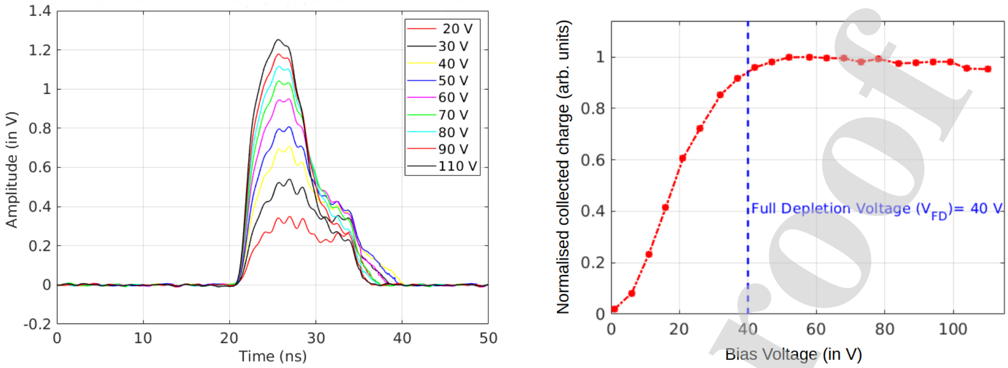

(a) (b)

Figure 5: Waveforms in AC-coupled sensor with red laser front illumination at different bias voltages (a) and the evolution of collected charge with IR laser at 1kHz frequency and an intensity of 45% at different bias voltages(b).

During the TCT study, we obtained signals from 20 to 110 V scans (Figure 5 (a)). In Figure 5 (b) the saturated CCE is indicating a full depletion voltage V_{fd} of about 40 V. The leakage current was about 10 µA under the IR laser illumination condition. The TCT spatial scanning results are shown in Figure 6. The two scans show pixel sensors with $150 \times 100\,\mu$m pitch compatible with PSI46dig readout chip, and sensors with $50 \times 50\,\mu$m pitch designed for the RD53A ROC. Since the laser does not penetrate metal areas, the lowest amplitude in the scanned results is at the center of the metal. The bias lines and individual pixels are clearly visible which indicates that the TCT scan achieved a satisfying spatial resolution in the preliminary pixel scans.

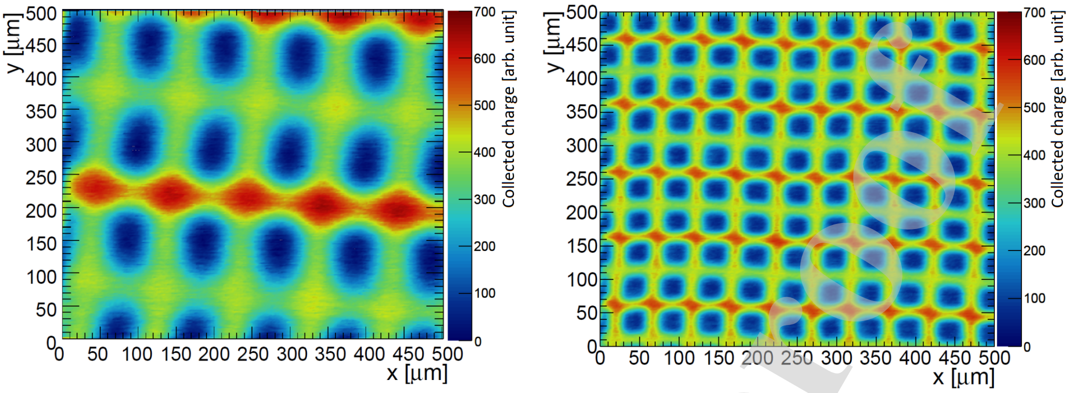

(a) (b)

Figure 6: TCT spatial scans and the corresponding peak current values: scanned area of $500 \times 500\ \mu m^2$ with PSI46dig geometry (a) and RD53A geometry (b).

4. Detector tests with radioactive sources

For evaluating the functionality of our AC-coupled pixel detectors, we followed the testing protocol of the standard CMS pixel detector quality assurance tests. Two fully assembled detectors, one with an implanted bias line and one with a metal bias line, were then exposed to radiation for testing the detector response. We used a measurement setup that is located in the Detector Laboratory at HIP. The calibration isotope Am-241 with its characteristic gamma emissions at 59.5 and 26.4 keV was used. The detectors were each connected to a printed circuit board (PCB) via wire bonds from the contact pads on the ROC. The PCB holding the detector was then connected through an adapter card via a 68 pin ribbon cable to the CMS detector test board (DTB). We used the pXar readout software for quality assurance and data collection [20]. The concept of the CMS based pixel sensor read-out and related terminology are described in detail in [21]. The distance between source and sample was 3 cm. During the measurement, a 40 V negative bias was applied to the back plane of the detector for full depletion. Typically, testing of the pixel unit cells (PUCs) requires a signal calibration, mainly for the timing of the trigger. The working point with optimal values are chosen from the center value of the tornado-plot in a VthComp vs CalDel mapping [21]. In pXar and the PSI46dig ROC, units of calibration charges (Vcal) are used, where 1 Vcal corresponds to 50 electrons.

During the spectra measurements, a Vcal trimming value was chosen between 100 to 120 in the pXar software. Although at trimming values of 65 - 80 we started to see the detector responding, at higher values noisy pixels are reduced significantly. In Figure 7 the effect of the trimming values is clearly seen. Figure 7 (a) shows a recorded Am-241 spectrum of the detector with the metal bias line at trimming value of 65 Vcal and Figure 7 (b) at trimming value of 100. It has to be noted that for the AC-coupled pixel detectors higher trimming values are needed compared to standard DC-coupled CMS pixel detectors, that show good results with values around 35 that correspond to 1750 electrons as lower threshold for signal processing of the PUCs [22].

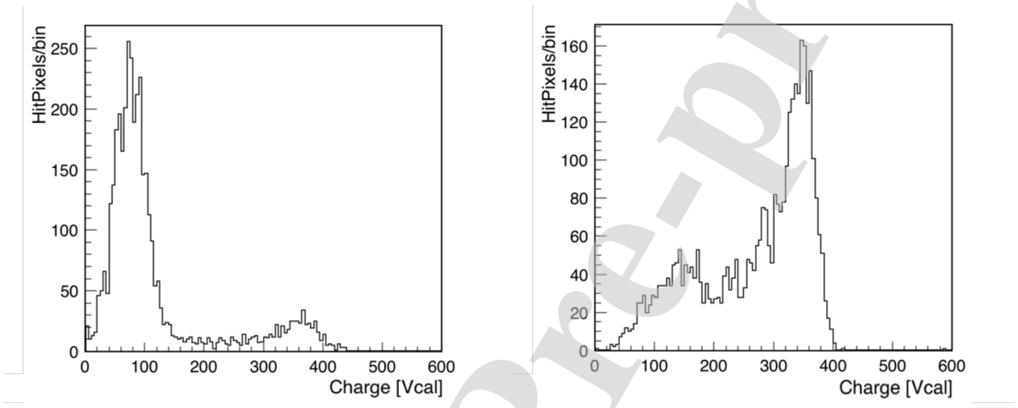

(a) (b)

Figure 7: (a) Pixel detector trimmed to a threshold of 65 Vcal, (b) the same detector trimmed to 100 Vcal.

The reason for that could be the baseline noise of the AC-coupled. In our pixel detector, the AC-coupled pixels act as a high pass RC-filter, hence less noise from the Si bulk leakage current would be expected [23]. However, the noise is affected by the total input capacitance per pixel, which is is dominated by the comparatively high coupling capacitance. Regarding this, it should be noted that the PSI46dig ROC was not developed and optimized for capacitive coupled pixel sensors. We suspect that the observed noise might be caused by the specification limits of the PSI46dig read out chip [24, 25]. This issue will be addressed in further studies.

Interesting is the comparison of both detectors under testing shown Figure 8. On the top, one can see the Am-241 spectrum recorded by the detector with the implanted bias line, and on the bottom by the detector with the metal bias line. The measurement conditions were otherwise equivalent. The spectrum of the detector with the implanted bias line, in figure 8 on top, shows approximately 10 % lower position of the 59.5 keV gamma peak in terms of Vcal. Also visible is a lower energy resolution as the 59.5 and the 26.4 keV peaks are not separable. This may indicate that we have a drain of charge into the bias ring through charge collection to the bias line implant, which leads to lower collected charge as well as poorer energy resolution.

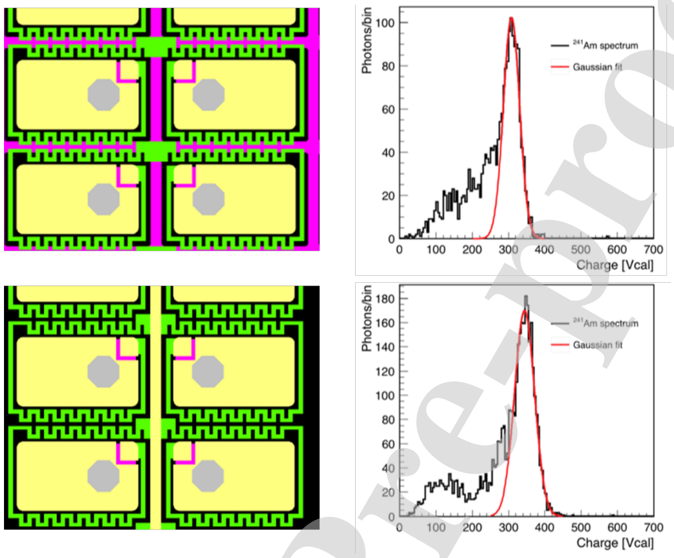

Figure 8: Left: Layouts of different bias line configurations in the mask, right: Am-241 spectra of pixel sensors with different bias line configurations. A shift in the centroid channel of the main peak is visible.

In figure 9 (a) an Am-241 spectrum is shown, recorded with the detector with the implanted bias line. The fitting of the plot uses the crystal ball function for the 59.5 keV gamma emission. On the left side of the photopeak, we observed the trend of a Gaussian function with a polynomial tail. One reason is that we do not have full absorption of the gamma-ray energy in the 320 µm thick sensor. The absorption efficiency of for example a 40 keV photon in Si is less than 5 %.

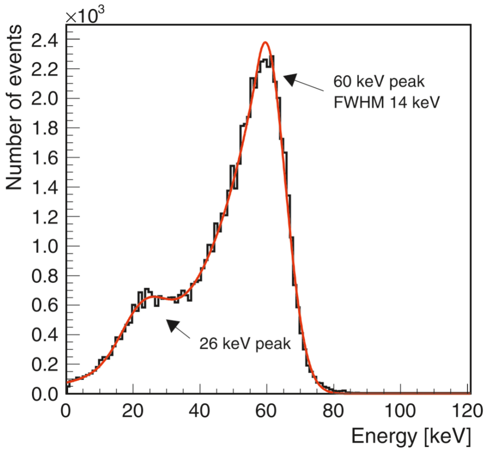

(a)

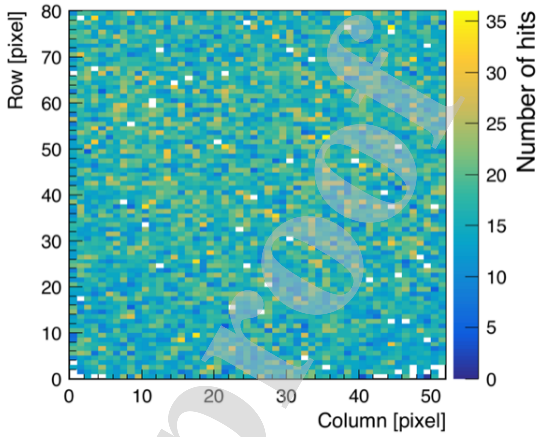

(b)

Figure 9: PSI46dig-geometry AC-coupled detector spectrum (a) and corresponding hit map (b).

However, for particle tracking applications the performance of our pixel detector in terms of energy resolution and signal-to-noise ratio is sufficient. The spectrum shows a 59.5 keV photopeak and a 26 keV k-line peak. The supplemental spectroscopic result qualitatively validates that our AC-coupled pixel detectors are functional. In Figure 9b the hit map for this measurement is shown. It shows that 99% of the individual pixels are responsive with a uniform behaviour, which is comparable to CMS pixel detectors.

5. Summary

We fabricated AC-coupled pixel sensors on 150 mm diameter MCz silicon wafers at Micronova Nanofabrication center in Finland. ALD grown thin film process was optimized and repeatedly applied in our process [26, 27]. We confirmed that individual pixels are effectively separated using scanning TCT. The TCT measurements showed full depletion at a voltage of 40 V. Therefore we can validate that our tailored material and processes are functional. Also, the fabricated detectors using hybrid technology on the PSI46dig ASIC with flip chip bump bonding technique was established. Fully assembled detectors were tested by measuring spectra of the radioactive isotope Am-241. According to our measurements, we have successfully demonstrated functional AC-coupled $n^+/p^-/p^+$ pixel detectors with ALD grown thin insulator film.

Acknowledgements

This study was partially funded by the Horizon 2020 ERA Chair project, grant agreement 669014 (Particle and Radiation Detectors, Sensors and Electronics in Croatia, PaRaDeSEC) and by Academy of Finland project number 314473, "Multi-spectral photon-counting for medical imaging and beam characterization". J. Ott acknowledges funding from the Viljo, Yrjö and Kalle Väisälä Foundation of the Finnish Academy of Science and Letters. Detector fabrication was performed in the cleanroom facilities of Micronova Nanofabrication Centre in Espoo, Finland, within the OtaNano research infrastructure. The authors are grateful to Dr. Eija Tuominen, coordinator of the Detector Laboratory at Helsinki Institute of Physics and University of Helsinki Department of Physics, for providing the environment for electrical measurements.

References

[1] G. Darbo, The ATLAS pixel detector, Nuclear Physics B - Proceedings Supplements 78 (1-3) (1999) 263–268. doi:10.1016/S0920-5632(99)00555-1.

[2] W. Erdmann, The CMS pixel detector, Nucl. Instrum. Methods Phys. Res., A 447 (1-2) (2000) 178–83.

[3] CMS Collaboration, The phase-2 upgrade of the CMS tracker, Tech. Rep. CERN-LHCC-2017-009. CMS-TDR-014, CERN, Geneva (2017).

[4] J. Härkönen, J. Ott, M. Mäkelä, T. Arsenovich, A. Gädda, T. Peltola, E. Tuovinen, P. Luukka, E. Tuominen, A. Junkes, J. Niinistö, M. Ritala, Atomic Layer Deposition (ALD) grown thin films for ultra-fine pitch pixel detectors, Nuclear Inst. and Methods in Physics Research, A 831 (2016) 2–6.

[5] J. Härkönen, E. Tuovinen, P. Luukka, E. Tuominen, Z. Li, p+/n−/n+ Cz-Si detectors processed on p-type boron-doped substrates with thermal donor induced space charge sign inversion, IEEE Transactions on Nuclear Science 52 (5) (2005) 1865–1868. doi:10.1109/TNS.2005.856619.

[6] J. M. Sturm, A. I. Zinine, H. Wormeester, B. Poelsema, R. G. Bankras, J. Holleman, J. Schmitz, Imaging of oxide charges and contact potential difference fluctuations in atomic layer deposited Al_2O_3 on Si, Journal of Applied Physics 97 (6) (2005) 063709.

[7] P. Repo, H. Talvitie, S. Li, J. Skarp, H. Savin, Silicon surface passivation by Al_2O_3: Effect of ald reactants, Energy Procedia 8 (2011) 681–687.

[8] M. Leskelä, M. Ritala, Atomic layer deposition (ALD): from precursors to thin film structures, Thin Solid Films 409 (1) (2002) 138–146.

[9] G. Dingemans, M. Sanden, van de, W. Kessels, Influence of the deposition temperature on the c-Si Surface passivation by Al_2O_3films synthesized by ALD and PECVD, Electrochemical and Solid-State Letters 13 (3) (2010) H76–H79. doi:10.1149/1.3276040.

[10] J. Härkönen, V. Eremin, E. Verbitskaya, S. Czellar, P. Pusa, Z. Li, T. Niinikoski, The Cryogenic Transient Current Technique (C-TCT) measurement setup of CERN RD39 Collaboration, Nuclear Instruments and Methods in Physics Research Section A: Accelerators, Spectrometers, Detectors and Associated Equipment 581 (1) (2007) 347 – 350, VCI 20070. doi:10.1016/j.nima.2007.08.001.

[11] E. Fretwurst, V. Eremin, H. Feick, J. Gerhardt, Z. Li, G. Lindström, Investigation of damage-induced defects in silicon by TCT, Nuclear Instruments and Methods in Physics Research Section A: Accelerators, Spectrometers, Detectors and Associated Equipment 388 (3) (1997) 356–360, radiation Effects on Semiconductor Materials, Detectors and Devices. doi:10.1016/S0168-9002(97)00002-8.

[12] V. Eremin, Z. Li, Determination of the fermi-level position for nutron-irradiated high-resistivity silicon detectors and materials using the transient charge technique (TCHT), IEEE Transactions on Nuclear science 41 (6, 1) (1994) 1907–1912. doi:10.1109/23.340522.

[13] G. Kramberger, V. Cindro, I. Mandić, M. Mikuž, M. Zavrtanik, Effective trapping time of electrons and holes in different silicon materials irradiated with neutrons, protons and pions, Nuclear Instruments and Methods in Physics Research Section A: Accelerators, Spectrometers, Detectors and Associated Equipment 481 (1) (2002) 297 – 305. doi:10.1016/S0168-9002(01)01263-3.

[14] K.Gabathuler, PSI46 Pixel Chip - External Specification, Tech. rep., accessed: February, 2020 (2005).

[15] J. Ott, A. Gädda, S. Bharthuar, E. Brücken, M. Golovleva, J. Härkönen, M. Kalliokoski, A. Karadzhinova-Ferrer, S. Kirschenmann, V. Litichevskyi, P. Luukka, L. Martikainen, T. Naaranoja, Processing of AC-coupled n-in-p

pixel detectors on MCz silicon using atomic layer deposited aluminium oxide, Nuclear Instruments and Methods in Physics Research Section A: Accelerators, Spectrometers, Detectors and Associated Equipment 958 (2020) 162547, proceedings of the Vienna Conference on Instrumentation 2019. doi:10.1016/j.nima.2019.162547.

[16] J. Ott, A. Gädda, S. Bharthuar, E. Brücken, M. Golovleva, J. Härkönen, M. Kalliokoski, A. Karadzhinova-Ferrer, S. Kirschenmann, V. Litichevskyi, P. Luukka, L. Martikainen, T. Naaranoja, Detector processing on p-type MCzsilicon using atomic layer deposition (ALD) grown aluminium oxide, talk:33rd RD50 Workshop, 26.-28.11.2018.

[17] Particulars, advanced measurement systems, http://particulars.si/index.php, accessed: January, 2018.

[18] G. Kramberger, D. Contarato, How to achieve highest charge collection efficiency in heavily irradiated position-sensitive silicon detector, Nuclear Instruments and Methods in Physics Research Section A: Accelerators, Spectrometers, Detectors and Associated Equipment 560 (1) (2006) 98–102.

[19] Z. Li, M. Bruzzi, V. Eremin, J. Härkönen, J. Kierstead, P. Luukka, D. Menichelli, Tuominen, E. Tuovinen, E. Verbitskaya, Gamma radiation induced space charge sign inversion and re-inversion in p-type MCZ Si detectors and in proton-irradiated n-type MCZ Si detectors, Nuclear Instruments and Methods in Physics Research Section A: Accelerators, Spectrometers, Detectors and Associated Equipment 552 (1) (2005) 34–42. doi:https://doi.org/10.1016/j.nima.2005.06.003.

[20] H. P. Simon Spannagel, Beat Meier, The pxarCore Library - Technical Documentation, Reference Manual, and Sample Applications, Tech. Rep. CMS NOTE -2016/001, CERN (2016).

[21] S. Simon, The pXar Data Acquisition and Calibration Framework. In: CMS Pixel Detector Upgrade and Top Quark Pole Mass Determination, Springer, Cham Print, 2017. doi:10.1007/978-3-319-58880-3-6.

[22] D. Hits, A. Starodumov, The CMS pixel readout chip for the phase 1 upgrade, Journal of Instrumentation 10 (05) (2015) C05029–C05029. doi:10.1088/1748-0221/10/05/c05029.

[23] J. Härkönen, E. Tuovinen, P. Luukka, A. Gädda, T. Maenpaa, E. Tuominen, T. Arsenovich, A. Junkes, X. Wu, Z. Li, Processing of n+/p−/p+ strip detectors with atomic layer deposition (ALD) grown Al_2O_3 field insulator on magnetic Czochralski silicon (MCz-si) substrates, Nuclear Instruments and Methods in Physics Research Section A: Accelerators, Spectrometers, Detectors and Associated Equipment 828 (2016) 46–51. doi:10.1016/j.nima.2016.04.069.

[24] H. Spieler, Introduction to Radiation Detectors and Electronics V.3. Semiconductor Detectors - Resolution and Signal-to-Noise Ratio, Tech. rep., accessed: February, 2020 (1999).

[25] H. Spieler, Front-end electronics and signal processing, Proceedings of the First ICFA School at the ICFA Instrumentation Center in Morelia 674 (2003) 76–100. doi:doi.org/10.1063/1.1604074.

[26] J. Ott, T. P. Pasanen, A. Gädda, M. Garín, K. Rosta, V. Vähänissi, H. Savin, Impact of doping and silicon substrate resistivity on the blistering of atomiclayerdeposited aluminium oxide, Applied Surface Science 522 (2020) 146400. doi:10.1016/j.apsusc.2020.146400.

[27] J. Ott, T. P. Pasanen, P. Repo, H. Seppänen, V. Vähänissi, H. Savin, Passivation of DetectorGrade FZSi with ALD Grown Aluminium Oxide, physica status solidi (a) 216 (17) 1900309. doi:10.1002/pssa.201900309.